



HAL
open science

Evolution of LSPR of gold nanowire chain embedded in dielectric multilayers

Zakariae Oumekloul, S. Lahlali, A. Mir, Abdellatif Akjouj

► **To cite this version:**

Zakariae Oumekloul, S. Lahlali, A. Mir, Abdellatif Akjouj. Evolution of LSPR of gold nanowire chain embedded in dielectric multilayers. *Optical Materials*, 2018, 86, pp.343-351. 10.1016/j.optmat.2018.10.020 . hal-03185124

HAL Id: hal-03185124

<https://hal.science/hal-03185124>

Submitted on 18 Aug 2021

HAL is a multi-disciplinary open access archive for the deposit and dissemination of scientific research documents, whether they are published or not. The documents may come from teaching and research institutions in France or abroad, or from public or private research centers.

L'archive ouverte pluridisciplinaire **HAL**, est destinée au dépôt et à la diffusion de documents scientifiques de niveau recherche, publiés ou non, émanant des établissements d'enseignement et de recherche français ou étrangers, des laboratoires publics ou privés.



Distributed under a Creative Commons Attribution 4.0 International License

Evolution of LSPR of gold nanowire chain embedded in dielectric multilayers

Z. Oumekloul^{a,b,*}, S. Lahlali^{a,b}, A. Mir^a, A. Akjouj^b

^a *Laboratory for the Study of Advanced Materials and Applications (LEM2A), Physics Department, Faculty of Science, Moulay Ismail University, B.P. 11201, Zitoune, Meknes, Morocco*

^b *Univ. Lille, Department of Physics, UMR 8520 – Institute of Electronics, Microelectronics and Nanotechnologies, F–59650, Lille, France*

The objective of this paper is to improve the sensitivity and the performance of nano-sensors by using the simulation, which was done by finite element method in 2D plasmonic nanostructures. Meanwhile, the effects of geometric parameters of a hexagonal gold nanostructure, and the influence of two dielectrics Si_3N_4 and SiO_x were treated. In order to have better sensitivity, the nature and the thickness of a deposited dielectric were controlled. Whenever we change the geometric parameters of the metallic nanostructure, we see changes in nanoparticle's plasmonic response. Adjusting the theoretical curve to experimental LSPR curve allowed the geometry of the plasmonic interface to be fixed and evaluation of the change in the wavelength at resonance (λ_R) as a function of the SiO_x overlayers thickness. The theoretical data were compared with experimental results obtained on glass/Au nanowires/ SiO_x and glass/Au Nanowires/ Si_3N_4 interfaces.

1. Introduction

The terms “nanomaterial” and “nanostructured material” appeared in the early 90s, but the study and use of nanomaterials are older. The colloids are the first community of this functionalized state of matter. However, a colloidal system was rarely perceived as a material, but rather as a fluid with special properties. Michael Faraday already studied the manufacture of nanoparticles by colloidal chemistry in the 19th century in the 1850s [1]. Faraday was well aware that colloidal gold behave very differently from macroscopic grain size vis-a-vis the visible light.

Currently there is strong demand for bio-sensing devices based on surface plasmon resonance (SPR) of noble metal nanoparticles in specific silver and gold deposited on functionalized surfaces [2–17]. Optical properties of metallic nanomaterials are determined by a set of parameters such as the chemical composition of the substrate in which the metal is deposited, the size particles and form, as well as the environment surrounding these metal nanomaterials. The LSPR are very sensitive to modifications in the medium close the surfaces. The effects of the refractive index of the surrounding medium on the plasmonic band LSPR (Localized Surface Plasmon Resonance) have been studied for many years [17–20]. Schultz studied the influence of the refractive index of the surrounding single silver nanoparticles in various oils [21].

After adding oil, the color of silver nanoparticles is changed from blue to green, indicating a shift to red color. The color of the modified nanoparticles turns blue when removing the oil. In the same year, Van Duyne uses silver nanoparticles as probes for detecting the formation of a monolayer on the surface of the nanoparticles [22].

The nanosensors based on LSPR have several advantages for bio sensing since it presents high sensitivity by detecting changes in the refractive index with no label and is flexible for the detection of biomolecular interactions of nanoparticles [19,20,23–26]. On top of that, the detection is in real time and allows the use of micro fluidic systems, low cost and ease for the instrumental configuration. These benefits show that these nanosensors can be applied in a wide range of areas, such as the medical field [20,27–30], that of food security [31,32], or the one on the monitoring of the environment [19].

In this work, we will numerically simulate the optical response of metal nanoparticles by changing the peak LSPR wavelength, for a hexagonal geometry based on the Drude-Lorentz-model for gold deposited on a glass substrate. On one hand, our study is carried out according to different geometric parameters of this hexagonal structure, and on the other hand, it depends on the thickness of the dielectric layers of SiO_x and Si_3N_4 deposited above the gold nanoparticles. Calculations are performed using the finite element method (FEM), which solves Maxwell's equations. The aim of our work is not only to

* Corresponding author. Laboratory for the Study of Advanced Materials and Applications (LEM2A), Physics Department, Faculty of Science, Moulay Ismail University, B.P. 11201, Zitoune, Meknes, Morocco.

E-mail address: z.oumekloul@edu.umi.ac.ma (Z. Oumekloul).

improve the performance and sensitivity of future nanosensors, but also to control them by changing the settings of the geometry, and the nature and thickness of the dielectric deposited on the structure for better quality detection.

This paper is organized as follows: In section 2 we present the technique of the formation of gold nanowires on glass and covered by Si_3N_4 or SiO_x . Section 3 briefly the Lorentz – Drude model. Section 4 present the optical characterization of the structure and simulation. Sections 5, 6 and 7 study the effects of the geometrical parameters of the Au nanowires and dielectric layers on the plasmonic responses, respectively. The conclusion is presented in section 8.

2. Experimental section

2.1. Formation of gold nanostructures on glass

Glass slides ($n = 1.51$) were cleaned in isopropanol and acetone in an ultrasound bath at room temperature, rinsed copiously with Milli-Q water, and dried under a stream of nitrogen. The clean substrates were transferred into an evaporation chamber. Gold nanostructures deposition was carried out by thermal evaporation of 4 nm thick gold films using MEB 550 S. Postdeposition annealing of the Au-covered slides was carried out at 500 °C for 1 min under nitrogen atmosphere, using a rapid thermal annealer (Jipelec Jet First 100). The reproducibility of the Au evaporation was evaluated by measuring the LSPR signals of a batch of 8 samples. The standard deviation in the wavelength (λ_R) and maximum absorption (I_{max}) is typically 2 nm and 0.02 abs units, respectively.

2.2. Deposition of dielectric overlayers

2.2.1. SiO_x

SiO_x overlayers were deposited on glass coated with Au nanostructures (glass/Au NWs) by plasma-enhanced chemical vapor deposition in a Plasmalab 800 Plus at a pressure of 0.005 Torr for 1 h. The growth conditions used were as follows: substrate temperature, 300 °C; gas mixture, SiH_4 (5% in N_2) and N_2O (the gas flow was 150 and 700 sccm for SiH_4 and N_2O , respectively); total pressure in the reactor, 1 Torr; and power, 20 Watt at 13.56 MHz. Under these experimental conditions, the deposition rate was 68.1 nm/min and the silica films display a refractive index $n = 1.45$. A total thickness of 300 nm was deposited and the thinner films were obtained by etching the SiO_x layer.

2.2.2. Si_3N_4

Si_3N_4 overlayers were deposited on glass coated with Au nanostructures by plasma-enhanced chemical vapor deposition in a Plasmalab 800Plus. The growth conditions used were as follows: substrate temperature, 200 °C; gas mixture of SiH_4 (5% in N_2) at 360 sccm gas flow, NH_3 at 20 sccm; total pressure in the reactor 1 Torr; power:

10 W at 13.56 MHz. Under these experimental conditions, the deposition rate is 7.2 nm/min and the films display a refractive index of $n = 2.01$. A total thickness of 300 nm was deposited and the thinner films were formed by etching of the Si_3N_4 layer.

2.2.3. Etching of the Si_3N_4 and SiO_x layers

The Si_3N_4 and SiO_x films are etched by a reactive ion etching (RIE) process using a gas mixture plasma in a RIE etching Plasmalab 80plus equipped with a laser interferometer (Jobin Yvon) at 670 nm. The etching rate was calibrated using two separate techniques. First, the etching rate was estimated within the plasma chamber by an interferometer on a Si_3N_4 and SiO_x layer on plane silicon. Then, the etching rate was estimated by ellipsometry measurements. The etching rate is 48 nm/min for Si_3N_4 using the following etching parameters: gas mixture SF_6 and Ar at 20 and 10 sccm gas flow, respectively, 50 W forwarded power, and 10 mTorr chamber pressure. The etching rate is 27.2 nm/min for SiO_x using the following etching parameters: gas mixture CHF_3 and CF_4 at 20 sccm gas flow each, 180 W forwarded power, and 50 mTorr chamber pressure.

2.3. Instrumentation

2.3.1. UV-vis spectrometer

Absorption spectra were recorded with a Perkin-Elmer Lambda UV/vis 950 spectrophotometer in cuvettes of 10 mm dimension. The wavelength range was 400–800 nm.

2.3.2. Scanning electron microscopy (SEM)

SEM images were obtained with an electron microscope ULTRA 55 (Zeiss) equipped with a thermal field emission emitter and a high-efficiency In-lens SE detector.

2.3.3. Ellipsometry

Spectroscopic ellipsometry data in the visible range were obtained with a UVISSEL Jobin Yvon Horiba Spectroscopic Ellipsometer equipped with DeltaPsi 2 data analysis software. The system acquired a spectrum ranging from 2 to 4.5 eV with 0.05 eV intervals. Data were obtained using an angle of incidence of 70° with the compensator set at 45° and fitted by regression analysis to a film-on-substrate model as described by their thickness and their complex refractive indices.

3. Theoretical model

Calculations are performed using the finite element method (FEM), which solves Maxwell's equations by discretizing space. Our calculation is performed in a two-dimensional (2-D) box (along x and y axes) with a propagation along the y axis. Perfect matching layer (PML) conditions are applied at the boundaries y of the box, to avoid reflections of outgoing waves. Along the x direction, the unit cell is repeated periodically

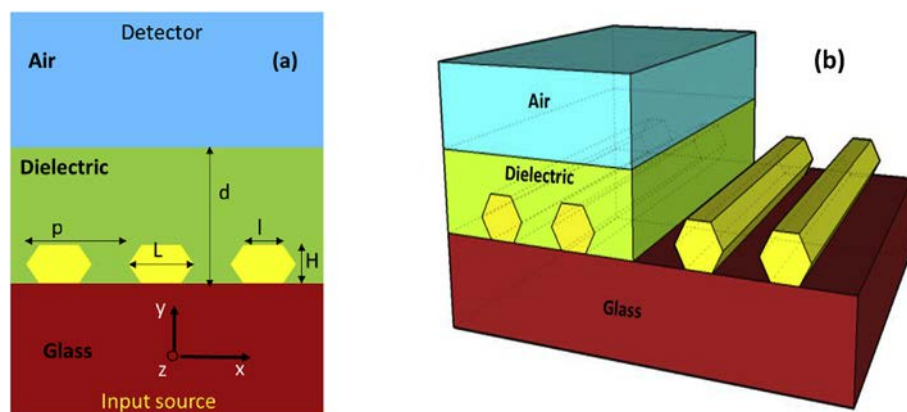


Fig. 1. (a) Schematic representation of the structure studied in this work. The gold nanowire is characterized by the height H and the diameters L and L . The inter-nanowire distance " p " is defined as the distance between two nearest neighboring gold nanowires. The input source is placed in the glass substrate and the detector in air. (b) 3D model of the plasmonic nanostructure. (For interpretation of the references to color in this figure legend, the reader is referred to the Web version of this article.)

(see Fig. 1) and the structure is supposed to be infinite along the z direction. Space is discretized in both x and y directions using a triangular mesh.

The input electromagnetic field, having TM polarization, is generated at the left part of the unit cell by a current source parallel to the x axis and having a planar profile along the x direction. The transmitted signal, probed at the end of the right part of the unit cell, is recorded as a function of frequency. All the transmission spectra are normalized with respect to the one corresponding to a structure without the array of metallic nanoparticles.

The plasmonic nanostructure studied in this work is constructed by the gold nanowires deposited on a dielectric substrate and the latter are covered by air (see Fig. 1). The metal of dielectric constant is described by the Lorentz–Drude model for described the frequency-dependent complex permittivity of metal (gold) the formula is given by Ref. [33]:

$$\varepsilon(\omega) = \varepsilon_\infty + \sum_{m=0}^M \frac{f_m \omega_p^2}{\omega_m^2 - \omega^2 + i\omega\Gamma_m} \quad (1)$$

where ε_∞ is the relative permittivity at infinite frequency, ω_p is the plasma frequency, ω_m , f_m , and Γ_m are, respectively, the resonance frequency, the strength, and the damping frequency of the m th oscillator. The Lorentz-Drude model uses $M = 5$ damped harmonic oscillators to describe the small resonances observed in the metal's frequency response. The values of the constants in Eq. (1) are given in Table 1. This model allows us to fit experimental data for the frequency-dependent dielectric constant of metals such as gold [33] including both the real and imaginary parts, with good agreement in the visible wavelength range ($400 < \lambda < 800$ nm).

4. Optical characterization of the structure and simulation

Fig. 1 displays the schematic illustration of the sensor configuration used for the theoretical studies. A layer of gold nanoparticles of diameters L and l , height h , and interparticle distance p are deposited on a transparent glass substrate ($n_{\text{SiO}_2} = 1.51$), coated with dielectric films of either SiO_x ($n_{\text{SiO}_x} = 1.45$) or Si_3N_4 ($n_{\text{Si}_3\text{N}_4} = 2.01$) and covered with a non-absorbing medium such as air with $n_{\text{air}} = 1$.

The hexagonal gold nanowire (NW) used in this nanostructure is characterized by its height H , the two diameters L and l , as well as the period p (see Fig. 1). During the study, we take into account a normal incidence of the incident electromagnetic field on the type of excitation, and we vary the wavelength in the visible range in order to detect the LSPR at the metal structure by modifying one of the previously defined geometrical parameters. Käll et al. [34], studied the LSPR frequency variation in function of the thickness of layers of tricosenoic acid 22 (a dielectric with a refractive index $n = 1.53$). In this study, the thickness of the acid tricosenoic-22 deposited on the considered nanostructures varies from 0.0 to 340 nm [34]. The layers of dielectric are deposited on a SiO_2 substrate, upon which two types of nanostructures have been studied experimentally. A random network of metallic gold nano-discs then a random network of air nano-holes perforated in a gold film with a thickness of 20 nm, deposited on SiO_2 . A similar study was carried out with gold nanostructures deposited on SiO_2 substrate. The layers of dielectric deposited on the metallic nanoparticles were SiO_x material

Table 1

The gold parameter values for Drude – Lorentz model [23].

Oscillateur m	f_m	ω_p (rad. s^{-1})	ω_m (rad. s^{-1})	Γ_m (rad. s^{-1})
0	0.76	$1.37188 \cdot 10^{16}$	0	$8.05202 \cdot 10^{13}$
1	0.024	$1.37188 \cdot 10^{16}$	$6.30488 \cdot 10^{14}$	$3.66139 \cdot 10^{14}$
2	0.01	$1.37188 \cdot 10^{16}$	$1.26098 \cdot 10^{15}$	$5.24141 \cdot 10^{14}$
3	0.71	$1.37188 \cdot 10^{16}$	$4.51065 \cdot 10^{15}$	$1.32175 \cdot 10^{15}$
4	0.601	$1.37188 \cdot 10^{16}$	$6.53885 \cdot 10^{15}$	$3.78901 \cdot 10^{15}$
5	4.384	$1.37188 \cdot 10^{16}$	$2.02364 \cdot 10^{16}$	$3.36362 \cdot 10^{15}$

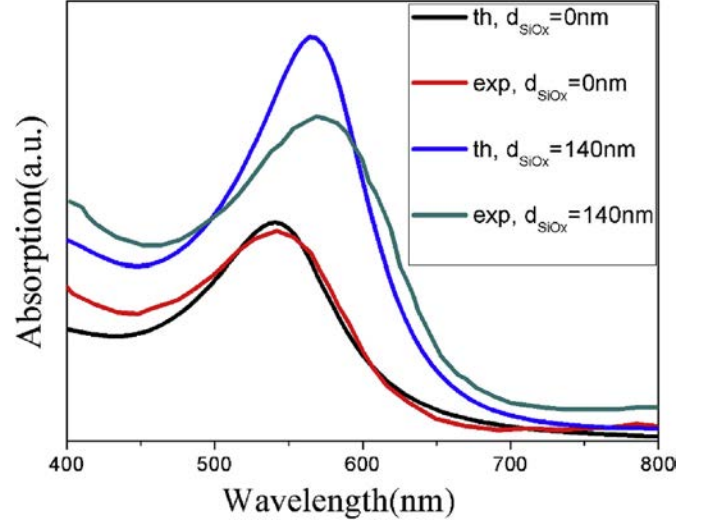


Fig. 2. Experimental and theoretical absorption spectra recorded on a glass/Au NWs interface without (red and black lines) and with a 140 nm thick SiO_x layer coating (blue and green). Parameters used for model: $l = 28$ nm, $L = 33$ nm, $p = 80$ nm and $H = 15$ nm. (For interpretation of the references to color in this figure legend, the reader is referred to the Web version of this article.)

[35], and their thicknesses ranged from 0.0 to 300 nm. The displacement of the observed properties of LSPR peaks in this study showed a red shift which was used for a study of the hybridization of the DNA molecule. These results showed the simultaneous influence of the dielectric refractive index deposited on the nanoparticles and its thickness on the behavior of the optical response at the interface LSPR. Galopin et al. have recently made the same comparison by using rectangular nanorods 2D [13]. Based on their experience, one can note a rather random particle shape, which requires them to determine statistical uncertainty with the dimensions of the nanoparticles in the overall structure. Akjouj et al. found that the most probable values for l and a respectively 25 ± 8 nm in diameter and 16 to 8 nm inter-particle distance. For the third dimension which is the height H of the values obtained is 13.6 ± 3 nm [36]. However, to keep the shape of our hexagonal structure, requires that the parameter L is larger than l , we took in this case $L = l + 5$ nm. The parameters selected for our structure resulting from these statistical results and the values chosen are: $l = 28$ nm, $L = 33$ nm, $p = 80$ nm, $H = 15$ nm.

In Fig. 2, we compare the case where the thickness of the dielectric SiO_x deposited upon the metallic gold structures, whose thickness is $d = 140$ nm, as well as in the case where the gold metallic structure are in direct contact with air (no dielectric SiO_x) whose thickness is $d = 0$ nm. We note a strong absorption around $\lambda_R = 545$ nm for both experimental and theoretical peaks, this value corresponds to the wavelength resonance that is to say, the plasmons excitation mode. Furthermore, one can grant the slight shift in magnitude to the sensitivity of the structure due to better sensitivity of hexagonal structure. However, we can decrease or increase the theoretical amplitude by adjusting it in function of the structure parameters, allowing to the experimental and theoretical results to be very close. In the second case we note a strong absorption in the vicinity of the wavelength resonance $\lambda_R \approx 568$ nm for both theoretical and experimental peaks, this value shows a shift towards the higher wavelengths of the absorption peak (almost a displacement of 23 nm in the visible band for a thickness of 140 nm) compared to case where $d = 0$ nm. This shows sensitivity of the structure to the displacements of the absorption peak for dielectric environment. The results obtained show a good agreement in terms of wavelength resonance. However there is a small difference in amplitude and the width of the peaks, which is due to a number of considerations including the comparison of a real system consisting of particles with

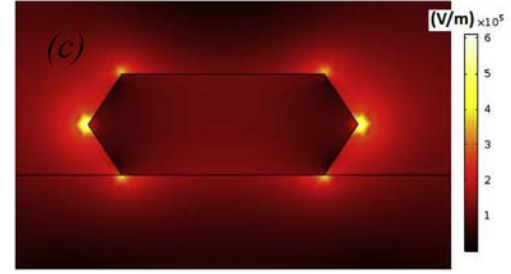
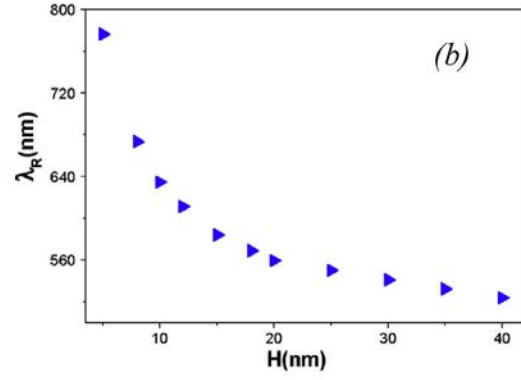
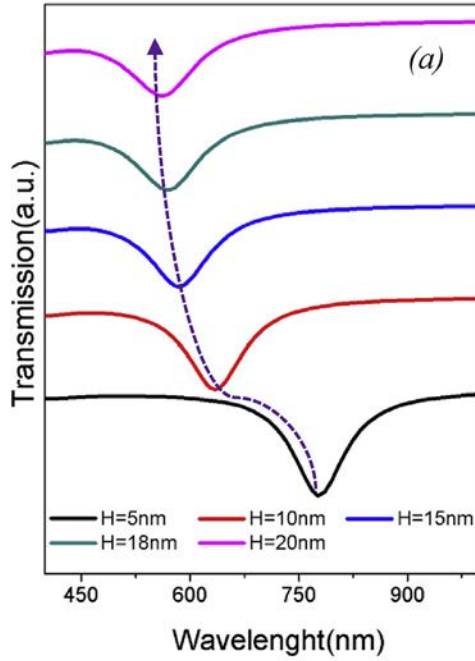


Fig. 3. (a) The transmission coefficient for a thickness $d = 140$ nm of SiO_x deposited on the gold hexagonal structure (dielectric constant calculated by the Drude-Lorentz model) equal for TM polarization. (b) Evolution of LSPR λ_R peak versus the height H . (c) The field map shows the distribution of the complex electric field amplitude for the resonance appearing in the spectrum for $H = 15$ nm ($\lambda_R = 584.07$ nm). (For interpretation of the references to color in this figure legend, the reader is referred to the Web version of this article.)

unequal sizes and ready for various use in a 3D simulation performed in 2D model described by a metal structure hexagonal according to the model of Drude-Lorentz.

5. Influence of the geometrical parameters on plasmons response

The modification of the geometric parameters of the metal structure (hexagonal) causes a change in the optical response of these nanoparticles. In this paragraph, we will focus on the changes caused by these geometric parameters. We admit the following values: $l = 30$ nm, $L = 40$ nm, $p = 80$ nm, $H = 15$ nm, and each time, a parameter is varied, we keep the values of the others constant.

5.1. The influence of the parameter H

Fig. 3-a shows the variation of the transmission coefficient for $H = 5, 10, 15$ and 18 nm with a thickness of SiO_x $d = 140$ nm deposited on the gold hexagon. Calculations Data: $L = 40$ nm, $l = 30$ nm, $p = 80$ nm, the substrate index $n = 1.51$, (constant thickness equal to 140 nm).

We noticed a displacement toward lower wavelengths with increasing H , accompanied by a decrease in the amplitude which shows high sensitivity for low heights especially for $H = 5$ nm (almost -7 dB). The minimum of the transmission coefficient corresponds to the resonance wavelength at which the incident wave is coupled to free electrons of metal particles, creating plasmons at the interface $\text{SiO}_2/\text{Au}/\text{SiO}_x$.

Fig. 3(b) shows changing the plasmons resonant wavelength of the particles according to H . A strong quasi-hyperbolic decay is observed in the resonance wavelength from 780 nm to 560 nm when the height of particles vary from 5 nm to 20 nm, and it continues to be smaller but significant for a variation of the wavelength from 560 nm to 525 nm when H ranges from 20 nm to 40 nm.

5.2. The influence of the parameter p

In this section, we will study the influence of the frequency p over plasmonic resonance by calculating the transmission coefficient for TM polarization. The period of structure is a very important parameter as it depends on the resonance related to the excitation of surface plasmons and describes the dipolar interactions in between particles at nanometre's level.

The calculation data are: $L = 40$ nm, $l = 30$ nm, $H = 15$ nm for $p = 45, 50, 60, 70, 80$ and 90 nm. It is therefore possible to see the influence of the geometry of the structure, by varying p , one can easily see the effect on the transmission spectrum for a TM polarization. Fig. 4(a) presents the transmission spectrum versus the wavelength. Gradually, as the particles approach each other, the optical behavior of structure becomes increasingly sensitive; when the particles approach, $p = 45$ nm, it shows a strong absorption of incident energy (-15 dB). This indicates that each dipole (metal structure) is subjected to an electric field resulting from the sum of the incident field and local fields produced by each of the neighboring dipole, and when the inter-particle distance is small, the mutual influence of particles has a strong coupling which makes the area more sensitive, for a better detection. The symmetric and homogenous charge distributions on both the left and right borders of the nanoparticle (see below Fig. 4 (a)) represent a quite evident consequence of the mode excitation for $p = 45$ nm induced by the TM wave.

There is a drop in the resonant wavelength from 720 nm to 582 nm (138 nm decrease), when p vary from 45 nm to 80 nm [see Fig. 4(b)]. Then there is a low decrease, from 582 nm to 580 nm, where p ranges from 80 nm to 90 nm. For low coupling between the metallic nanostructures, p variation has almost no effect on the response of the particles. So, compared to other structures considered as the gold ribbon a better result can still be seen. This structure concentrates and absorbs the field in a very sub-wavelength volume, which represents a crucial interest for detection. Fig. 4(c) represents the electric field distribution at the incident wavelengths (of the dips) $\lambda_R = 718$ nm. At these wavelengths, the field is trapped in the nanoparticle cavity and does not

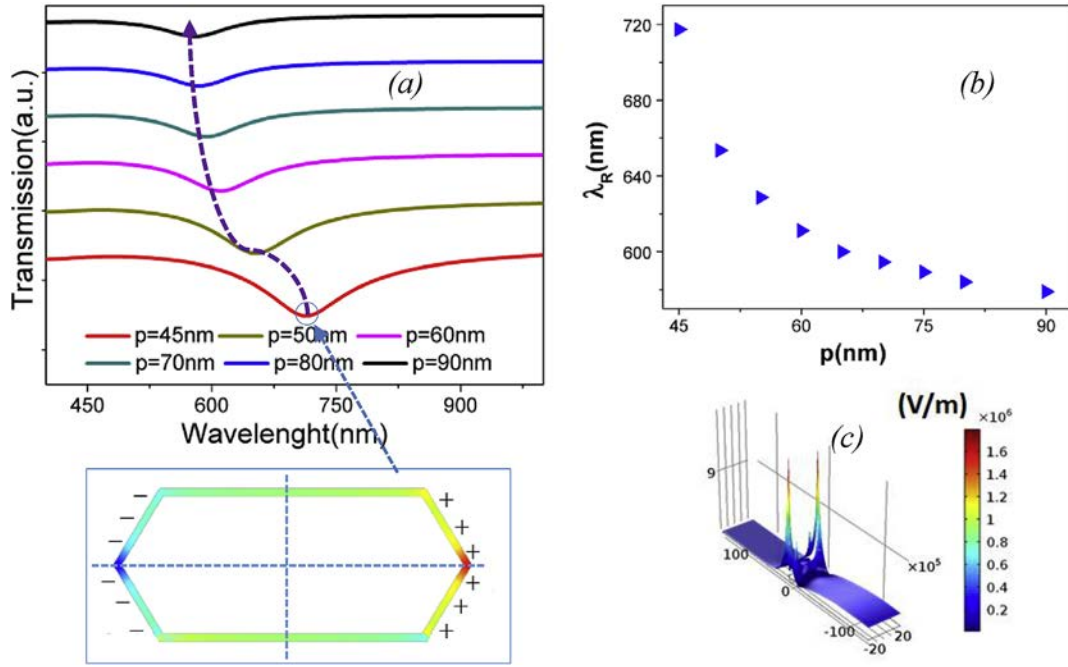


Fig. 4. (a) Transmission coefficient for a thickness $d = 140$ nm SiO_x deposited on hexagonal gold structure (dielectric constant calculated by the Drude-Lorentz model) equal for TM polarization with surface charge of dipolar mode at resonance frequency ($\lambda_R = 717.9$ nm). (b) Evolution of the resonance wavelength as a function of p. (c) Presents the electric field map at $p = 45$ nm ($\lambda_R = 717.9$ nm). (For interpretation of the references to color in this figure legend, the reader is referred to the Web version of this article.)

propagate in the system.

5.3. The influence of the parameter L

The effect of parameter L will be observed in the transmission spectrum for TM polarization while keeping these constant parameters: $H = 15$ nm, $L = 35$ nm $p = 80$ nm for $L = 40, 45, 50, 55, 60$ and 65 nm.

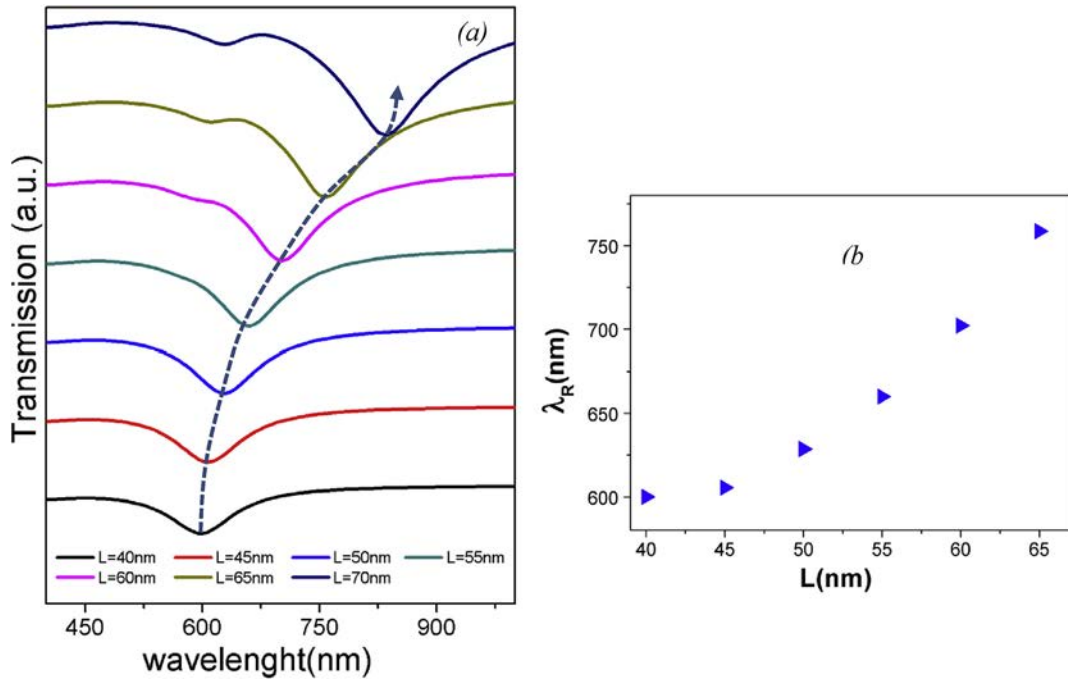


Fig. 5. a-Transmission of the TM polarized wave with a normal incident on the surface metal. Calculated for a network of hexagon metal gold for constant values of $H = 15$ nm, $l = 35$ nm and $p = 80$ nm b- Evolution of the resonance wavelength as a function of L. (For interpretation of the references to color in this figure legend, the reader is referred to the Web version of this article.)

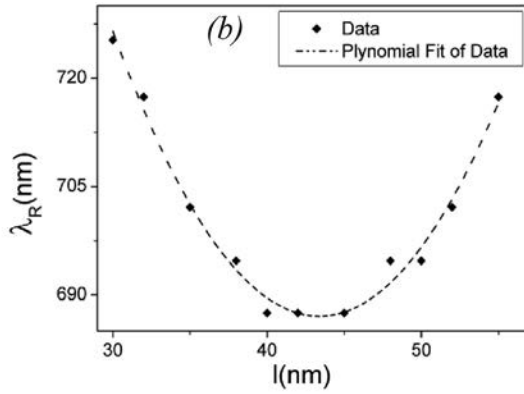
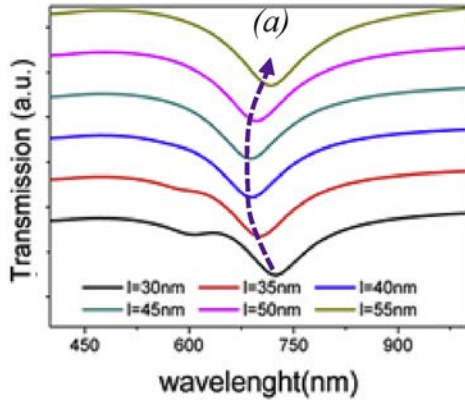


Fig. 6. (a) The transmission evolution of wavelength when l taking the values 30, 35, 40, 45, 50 and 55 nm. (b) Evolution of the resonance wavelength as a function of l .

large exchange surface on the dielectric/metal interface. Starting from 60 nm, we observe the appearance of another peak around 600 nm. The latter appeared due to the change of the charging orientation of the dipolar mode.

Fig. 5-b shows the evolution of the resonance wavelength depending on L , which links it directly to the behavior of the resonance wavelength of the plasmons. Indeed, it is noticed, between 40 nm and 50 nm, that the plasmon resonance wavelength is growing a non-linear manner with L . Between 50 nm and 60 nm, of the plasmon resonance is growing almost linearly with L , which shows a reasonable agreement with the result obtained for the parameter p , since by increasing L , nanostructures approach and coupling remain increasingly strong, leading on the one hand to a high sensitivity. On the other hand to a movement toward the infrared, which presents an advantage to the biosensor in the infrared range.

5.4. The influence of the parameter l

Likewise, it is possible to study the influence of the transmission curve (Fig. 6) for TM polarization. Thus, the choice of the other parameters is given by: $L = 60$ nm, $H = 15$ nm, $p = 80$ nm for the values $l = 30, 35, 40, 45, 50$ and 55 nm.

Fig. 6(a) shows that parameter l has great influence on the peaks amplitude, because the displacement does not matter between the values. There is a displacement of 23 nm for $l = 30$ nm–35 nm, 14.5 nm for $l = 35$ nm–40 nm, 0 nm for $l = 40$ nm–45 nm, 7.5 nm for $l = 45$ nm–50 nm and 22 nm $l = 50$ nm–55 nm. For $l = 30$ nm and 55 nm, we have almost the same resonance wavelength (725 nm and 717 nm respectively), but the second value is better in terms of amplitude. Fig. 6(b) shows the evolution of l on the resonance wavelength of each peak as a function of l .

Based on Fig. 6(b) an almost linear decrease is observed between $l = 30$ nm to 40 nm, for this interval, the peaks move to the short lengths wave and remain constant between 40 nm and 45 nm then grow to larger wavelengths from 45 nm to 55 nm. As for the amplitude, there is a gradual improvement due to the width of l which is in direct contact with the dielectric making better sensitivity for this hexagonal structure.

According to the observation of the various figures, we see that the resonance shape peaks and the value of the resonant frequency evolve according to the geometric parameters choice of the hexagonal structure. This give better results for the sensitivity of biosensors.

6. Effect of dielectric layers on the plasmons response

In sections 6.1 and 6.2 of this part, we will focus on the effect of the refractive index and the thickness of dielectric medium deposited on top of the metal structure. The two dielectrics studied are silicon oxide

SiO_x whose refractive index is $n_{SiO_x} = 1.45$ and the silicon nitride Si_3N_4 whose refractive index is $n_{Si_3N_4} = 2.01$. They are widely used experimentally for their poor absorption and can protect nanoparticles from morphological changes when applied to aqueous solutions or organic solvents. The choice of these two dielectric is not arbitrary that is why we will study them:

- ✓ The refractive index of the substrate is higher than that of the dielectric layer ($n_{SiO_2} > n_{SiO_x}$).
- ✓ The substrate refractive index is lower than that of the dielectric layer filed ($n_{SiO_2} < n_{Si_3N_4}$).

We used the following silicon oxide alloys and silicon nitride, deposited on metallic gold nanostructures immobilized to the glass, to study the behavior of the plasmons response and choose the best dielectric and the thickness to enhance the sensitivity of detection of the biosensor.

6.1. The effect of SiO_x

The effect of the thickness of SiO_x deposited on the hexagonal structure of gold is carried out when used in giving the thickness of the SiO_x layer the values $d = 20$ nm, 80 nm, 120 nm, 160 nm, 280 nm, while preserving the following parameters: $L = 40$ nm, $l = 30$ nm, $p = 80$ nm. Fig. 7 shows the curve of the transmission coefficient of an interface SiO_x -Air for TM polarization.

There is an oscillation in the resonance wavelength for a range of value of the thickness of the dielectric with a quite good sensitivity. These oscillations observed in the spectrum are due to coupling between the plasmons mode and the modes of a Fabry-Perot cavity connected to the presence of the oxide layer silicon SiO_x presented above the gold nanowire chain: Light incoming perform multiple round-trip within the cavity defined by SiO_x and SiO_2 , and partially spring at each reflection.

6.2. The effect of the Si_3N_4 dielectric overlayer thickness

When changing the SiO_x dielectric by the chemical compound of formula Si_3N_4 , the plasmons response of gold nanoparticles changes. Silicon nitride is a hard ceramic whose physical properties are maintained over a wide temperature range. Fig. 8 (a) shows the evolution of the transmission spectra versus wavelength of an interface Si_3N_4 /Air, depending on the thickness of the Si_3N_4 dielectric layers for values $d = 20$ nm, 80 nm, 120 nm, 160 nm and 280 nm, for TM polarization. The hexagonal gold nanowires have the following calculation parameters: $L = 40$ nm, $l = 30$ nm, $p = 80$ nm, with the index of the substrate $n_{SiO_2} = 1, 51$.

An increase in the amplitude is deduced, so a strong absorption

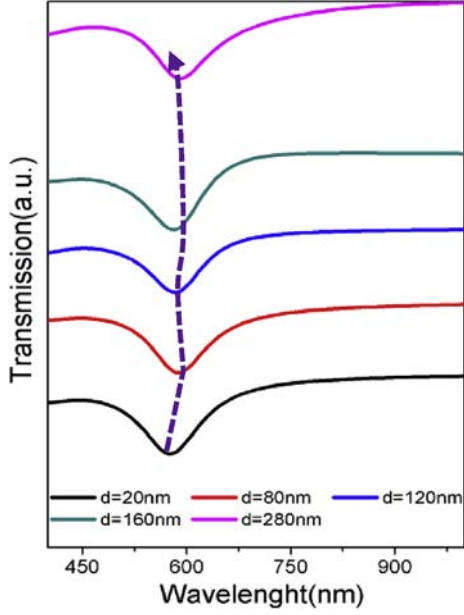


Fig. 7. Spectral shape and position of the LSPR peak of transmission depending on the thickness of SiO_x layer.

which improves the sensibility in an extraordinary way, which is doubled when compared to the SiO_x case, and also to the sensitivity of the structure studied in Fig. 8. Fig. 8(b) shows the change in λ_R as a function of Si_3N_4 thickness. It was predicted that the LSPR shift should saturate at $\Delta\lambda_R \approx m\Delta n \approx 46\text{nm}$ [27,28,37], where m is the refractive index sensitivity for the glass/Au interface ($m = \frac{\delta\lambda_R}{\delta n} = 90\text{nm}$) and Δn the change in the refractive index induced by the adsorbate. Van Duyne and co-workers explored experimentally the long-range distance dependence of LSPR nanosensors using self-assembled monolayers (SAMs) of 11-mercaptopundecanoic acid and Cu^{2+} ions absorbed on surface-confined noble metals nanoparticles [27]. It was found that the shift of λ_R with increasing adsorbate thickness is nonlinear and has a sensing range that is dependent on the composition, shape, width, and height of the nanoparticles. The use of atomic layer deposition of Al_2O_3 enabled, in addition, the study of both the long- and short-range distance dependence of the LSPR nanosensors [37,38]. At short distances

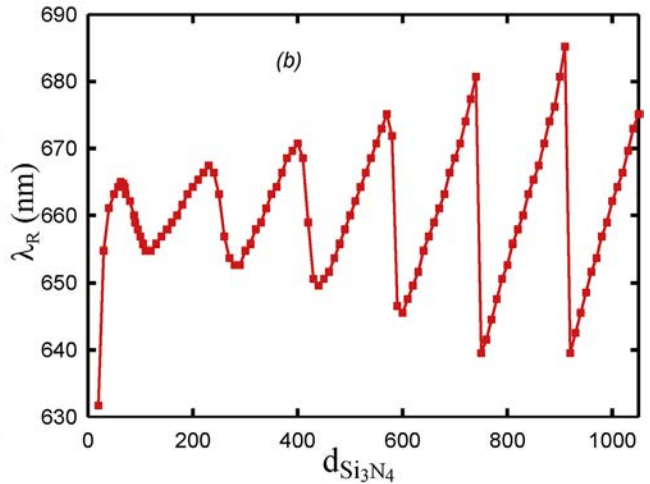
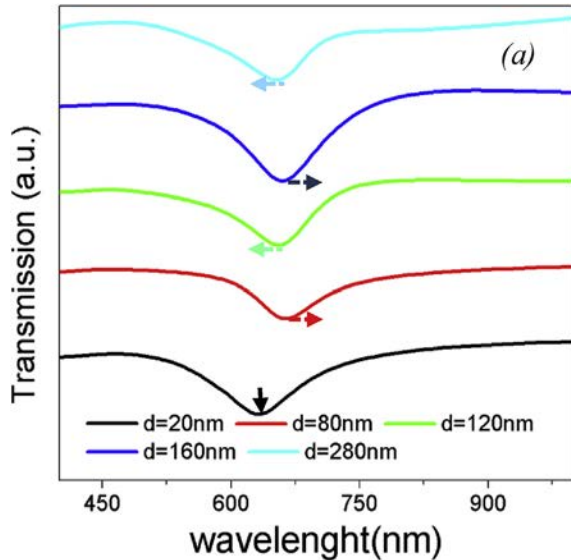


Fig. 8. (a) Evolution of the transmission spectrum vs the wavelength corresponding to the structure of Fig. 1 for different values of the thickness of Si_3N_4 ; $d = 20\text{ nm}$, 80 nm , 120 nm , 160 nm , 280 nm . (b) Oscillation of resonance wavelength.

from the nanoparticles surface, the LSPR λ_R shift follows a steep linear slope, but as the distance from the nanoparticles increases, the curve bends over and eventually levels off once a saturation point is reached. This is clearly not observed for the interfaces under study.

Fig. 8(b) shows that the presence of a Si_3N_4 overlayer causes theoretically first a red shift until saturation at $d_{\text{Si}_3\text{N}_4} \approx 62\text{nm}$. In the range $62 < d_{\text{Si}_3\text{N}_4} < 115\text{nm}$ blue shift in λ_R is observed, followed by a red shift until $d_{\text{Si}_3\text{N}_4} \approx 230\text{nm}$. This oscillation extends until 1080 nm with a periodicity of $d_p = 168\text{nm}$ and with increasing amplitude at $d_{\text{Si}_3\text{N}_4} > 850\text{nm}$. The resonances (corresponding to the maximum of the amplitude of the oscillations) and the anti-resonances (corresponding to the minimum of the amplitude of the oscillations) are similar to the classical Fabry-Perot cavity. Moreover, the periodicity of the oscillation can be calculated by the equation $d_p = \lambda_R/2n$, where n is the refractive index of the dielectric layer [$d_p \approx \frac{664}{2 \times 2.01} = 165\text{ nm}$ (see Fig. 8(b))]. The oscillation is anharmonic and the plasmon shift is faster in the blue-shifting regions (e.g., 90 nm , 255 nm , etc.) than in the red-shifting regions (e.g., 20 nm , 185 nm , etc.). The results in Fig. 8(b) indicate that refractive index sensitivity increases with increasing distance (i.e., the particle are infinitely and increasingly more sensitive to layer thicknesses). Finally, let us notice that the dielectric deposited on the metallic gold nanostructure having a wide index relative to that of the substrate, leads to better results thanks to the sensitivity of the plasmonic response function of the thickness d . This structure absorbs the concentrated field in a volume with sub-wavelength, which represents a crucial interest for detection.

The calculated LSPR curves are corroborated by the experimental LSPR curves recorded on glass/Au nanowire coated with SiO_x of increasing thicknesses. Fig. 9 shows the obtained shift in λ_R together with the ones predicted through modeling. The square dots represent the theoretical results whereas the triangle-shaped dots corresponds to the experimental ones. For all the Si_3N_4 overlayer, the theoretical results agree with the experimental one.

7. Study of the sensitivity

The plasmonics LSPR nano-sensors works by variation of the resonance wavelength. It is clear that the plasmonic response of metallic nanoparticles is strongly depend on their size and shape. In addition, this dependence affects the importance of the spectral shift of the resonance, following the change in the refractive index of the medium located near the metal nanowires. We showed a high sensitivity of the

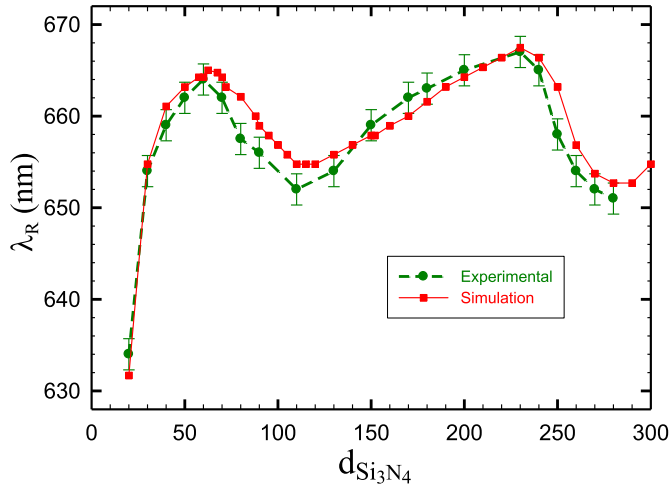


Fig. 9. Evolution of λ_R with the thickness of the Si_3N_4 overlayer; comparison of experimental (triangle-shaped dots) and theoretical (square dots) data.

metal nanoparticle plasmon response with different geometrical parameters of Au nanoparticles and/or refractive index of the dielectric deposited on the top of the Au nanoparticles. Fig. 1 show the proposed sensing structure, where the layer dielectric is on the top of Au nanowire. To qualify the performance of the proposed sensor, we compute a sensing S . The expression used to calculate the sensitivity is given by:

$$S = \frac{\Delta\lambda_R}{\Delta n},$$

where Δn is the variation of the refractive index between the dielectric (SiO_2) and one of the other substance used and $\Delta\lambda_R$ the variation of the resonance wavelength.

In the first part, we investigate theoretically the influence of the refractive index of the overcoating relative to the underlying substrate, supporting the metal nanostructures, on the sensitivity of the multi-layered interface for sensing. This is indeed a highly important parameter for the development of a sensitive LSPR interface. The structure studied here consists of gold nanowires of height $H = 15$ nm and the diameters $L = 40$ nm and $l = 30$ nm deposited on a SiO_2 substrate and coated with dielectric film with $d = 20$ nm (see Fig. 1). The lattice parameter $p = 80$ nm. Three different cases can thus be distinguished: (i) the refractive index of the substrate is higher than that of the deposited dielectric layer; (ii) the refractive index of the substrate is the same as that of the deposited dielectric layer; and (iii) the refractive index of the substrate is lower than that of the deposited dielectric layer. The interface is furthermore covered by a air. To obtained these three case, we use the following dielectrics: H_2O , C^6H_6 , ITO and Si_3N_4 and air as reference.

Table 2 presents a comparison of sensitivity between different dielectrics deposited on the Au nanowires. The thickness of the dielectric layer is $d = 20$ nm in all case studied here. We noticed that benzene has a very high sensitivity; it can be explained by the fact that the benzene has the same refractive index as the substrate (glass). In other words, because of the fact that the refractive index are the same, there is an absence of the interface between the substrate and the dielectric. In this

Table 2
Comparison table in sensitivity between different substances for hexagonal gold nanoparticles.

Dielectric	Refractive index	Sensitivity (nm/RIU)
Water	1.33	249.5
Benzene	1.50	607
ITO	2.00	406.5
Si_3N_4	2.01	415.7

case, the Fabry-Perot cavity mode disappears which is not the case for where the refractive index of the dielectric is different from the substrate refractive index [cases (i) and (iii)]. In the last case, when the refractive index of the over-layer is higher than substrate refractive index, the sensitivity is relatively good. In this situation, the oscillations cavity mode increases and coupled with plasmonic mode, however the existence of the interface between the substrate and the dielectric affects the sensibility because they reduce the confinement of the electric field supported by Au nanowires. From this model it emerged that the sensitivity exclusively depends on the LSPR band location and the refractive index of the dielectric. We conclude that the optimal sensitivity is obtained when the index of the overlayer is of the same nature as that the refractive index of the substrate.

In the second part, we compare the evolution of the sensitivity between different geometrical gold nanowires but with the same basic area (1500 nm^2). The sensitivity of the structures considered has been determined by identifying the position of the main resonance mode on their transmission spectra when the middle of the detection is air and Si_3N_4 . The structure studied here consists of gold nanowires of height $H = 25$ nm and the diameters $L = 80$ nm and $l = 40$ nm deposited on a SiO_2 substrate and coated by dielectric film with thickness $d = 30$ nm. In this study, we have used Si_3N_4 as a dielectric because the sensitivity of nanoparticles situated in a homogeneous host matrix (i.e. this situation correspond to the case where the refractive index of the substrate and the dielectric is the same) is independent of their shape [38]. The sensibility was also approximated in this study by $\Delta\lambda_{\text{LSPR}}/\Delta n$. We observe that the nanowire with the base in hexagonal form present a greater sensitivity than the other geometric shapes of the nanowire. The results are summarized in Table 3.

The origin of the high sensitivity of the infrared plasmon band is due to the high electrical field confinement between the Au nanostructures and due to the shape of the nanostructures itself. The hexagonal structure supports a strong localization of the electric field in the corners of the gold NPs that are numerous in our structure compared to others (we may well see it in the mapping of the field), In fact, the sensitivity of a plasmonic structure is also dependent on the location of the field around the nanoparticles at the resonance. The hexagonal geometry has 6 hot spots, two of which are in contact with the substrate, which generally has losses in terms of localized field intensity. We can draw the following conclusion; the exaltation of the electric field in the neighborhood NPs improves the sensitivity of the device. Additionally, the choice of the covering layer, which is accompanied by an index contrast with the substrate, amplifies the confinement of the electrical field due to interference created by the Fabry-Perot cavity.

The theoretical results obtained show that hexagonal nanowires is two time more sensitive than a triangular nanowire, three time more than a circular nanowire and 2.3 more sensitive than rectangular nanowire (see Table 3). These results will improve the performance of future nano-biosensors.

8. Conclusion

We have developed a theoretical study of optical properties of hexagonal gold metal nanoparticles, deposited on a glass substrate,

Table 3
Comparison table in sensitivity between circular, rectangular, hexagonal and triangular gold nanowires (the basic area of the nanowire = 1500 nm^2).

Geometry	Sensitivity
Circular 	202.0 nm/RIU
Rectangular 	270.3 nm/RIU
Triangular 	307.0 nm/RIU
Hexagonal 	620.8 nm/RIU

SiO_2 , upon one of the dielectric, SiO_x or Si_3N_4 by exploiting the resonance localized surface plasmons (LSPR) capable of detecting molecules at a nano-scale. In fact, the hexagonal structure is 2.3 times better than the rectangular because the sensitivity of the hexagonal is 621 nm/RIU, and thus way greater than the other structures. We have seen that the plasmons response of the hexagonal structure based on geometrical parameters showed better sensitivity than gold ribbon. This has improved the sensitivity of the interface, which allows us to have nano-sensors very sensitive in order to be more adequate to the biological and chemical detection. It was also seen that the resonance wavelength of the plasmons response manifest an oscillatory variation in function of the thickness of dielectric layers deposited on the particles. This phenomenon is interpreted in terms of the coupling of mode surface plasmons particles with those of the optical cavity, which consists of SiO_x , bounded on both sides of the detection medium and SiO_2 substrate. The same result was shown with Si_3N_4 , which has a contrast index greater with SiO_2 but slightly shifted towards longer wavelengths and with a better sensitivity. Significant efforts have been made experimentally in the last years to increase the sensitivity of the refractive index of the interface LSPR, but it seems necessary to wait a few years to see technical improvement, particularly with the new generation of detectors.

Acknowledgments

Z.O. and S.L. gratefully acknowledge the hospitality of the Institute of Electronics, Microelectronics and Nanotechnologies (IEMN), UMR CNRS 8520 and Department of Physics, University of Lille.

References

- [1] M. Faraday, Experimental relations of gold (and other metals) to light, Phil. Trans. R. Soc. Lond. January 1 (1857).
- [2] J. Li, C. Chen, L. Lagae, P. Van Dorpe, J. Phys. Chem. C 119 (2015) 29116–29122.
- [3] W.R. Erwin, R. Bardhan, J. Phys. Chem. C 120 (2016) 29423–29431.
- [4] M. Focsan, A.M. Craciun, M. Poataru, C. Leordean, A. Vulpoi, D. Maniu, S. Astilean, Sci. Rep. 7 (2017) 14240.
- [5] S.A. Maier, M.L. Brongersma, P.G. Kik, S. Meltzer, A.A.G. Requicha, H.A. Atwater, Plasmonics - a route to nanoscale optical devices, Adv. Mater. 13 (2001) 1501–1505.
- [6] T. Abhilash, M. Balasubrahmaniam, A. Patra, S. Kasiviswanathan, Appl. Phys. Lett. 104 (2014) 1–5.
- [7] S. Pillai, K.R. Catchpole, T. Trupke, M.A. Green, J. Appl. Phys. 101 (2007) 093105.
- [8] K.R. Catchpole, A. Polman, Appl. Phys. Lett. 93 (2008) 191113.
- [9] K.M. Mayer, J.H. Hafner, Chem. Rev. 111 (2011) 3828–3857.
- [10] S. Szunerits, R. Boukherroub, Chem. Commun. 48 (2012) 8999–9010.
- [11] O. Krupin, W.R. Wong, P. Beland, F.R.M. Adikan, P. Berini, J. Lightwave Technol. 34 (2016) 4673–4681.
- [12] J. Zhang, L. Zhang, W. Xu, J. Phys. D Appl. Phys. 45 (2012) 113001.
- [13] E. Galopin, J. Niedziolka-Jonsson, A. Akjouj, Y. Pennec, B. Djafari-Rouhani, A. Noual, R. Boukherroub, S. Szunerits, J. Phys. Chem. C 114 (2010) 11769–11775.
- [14] E. Galopin, A. Noual, J. Niedziolka-Jonsson, M. Jonsson-Nedziolka, A. Akjouj, Y. Pennec, B. Djafari-Rouhani, R. Boukherroub, S. Szunerits, J. Phys. Chem. C 113 (2009) 15921–15927.
- [15] S. Szunerits, S. Ghodbane, J. Niedziolka-Jonsson, E. Galopin, F. Klauser, A. Akjouj, Y. Pennec, B. Djafari-Rouhani, R. Boukherroub, D. Steinmuller-Nethl, J. Phys. Chem. C 114 (2010) 3346–3353.
- [16] S. Szunerits, V.G. Praig, M. Manesse, R. Boukherroub, Nanotechnology 19 (2008) 195712–195719.
- [17] N. Nath, A. Chilkoti, Anal. Chem. 76 (2004) 5370–5378.
- [18] K.M. Mayer, S. Lee, H. Liao, B.C. Rostro, A. Fuentes, P.T. Scully, C.L. Nehl, J.H. Hafner, ACS Nano 2 (2008) 687–692.
- [19] A.W. Murray, B. Auguié, L.W. Barnes, J. Phys. Chem. C 113 (2009) 5120–5125.
- [20] J. Homola, Surface Plasmon Resonance Based Sensors, Springer Series on Chemical Sensors and Biosensor/Methods and Applications vol. 4, Springer-Verlag Berlin, Heidelberg, 2006.
- [21] J.J. Mock, D.R. Smith, S. Schultz, Nano Lett. 3 (2003) 485–491.
- [22] A.D. Mcfarland, M.A. Young, J.A. Dieringer, R.P. Van Duyne, J. Phys. Chem. B 109 (2005) 11279.
- [23] E.M. Yeatman, Biosens. Bioelectron. 11 (1996) 635–649.
- [24] E.M. Larsson, J. Alegret, M. Käll, D.S. Sutherland, Nano Lett. 7 (2007) 1256–1263.
- [25] A.D. Mcfarland, M.A. Young, J.A. Dieringer, R.P. Van Duyne, Nano Lett. 3 (2003) 1057–1062.
- [26] W.P. Chen, J.M. Chen, J. Opt. Soc. Am. A 71 (1981) 189.
- [27] A.J. Haes, S. Zou, G.C. Schatz, R.P. Van Duyne, J. Phys. Chem. B 108 (2004) 109.
- [28] A.J. Haes, S. Zou, G.C. Schatz, R.P. Van Duyne, J. Phys. Chem. B 108 (2004) 6961.
- [29] A.J. Haes, L. Chang, W.L. Klein, R.P. Van Duyne, J. Am. Chem. Soc. 127 (2005) 2264–2271.
- [30] A.J. Haes, W.P. Hall, L. Chang, W.L. Klein, R.P. Van Duyne, Nano Lett. 4 (2004) 1029–1034.
- [31] B.A. Chromy, R.J. Nowak, M.P. Lambert, K.L. Viola, L. Chang, P.T. Velasco, B.W. Jones, S.J. Fernandez, P.N. Lacor, P. Horowitz, C.E. Finch, G. A Krafft, W.L. Klein, Biochemistry 42 (2003) 12749.
- [32] S. Yokogawa, S.P. Burgos, H.A. Atwater, Nano Lett. 12 (2012) 4349.
- [33] A.D. Rakic, A.B. Djuristic, J.M. Elazar, M.L. Majewski, Appl. Opt. 37 (1998) 5271.
- [34] T. Rindzevicius, Y. Alaverdyan, M. Kall, W.A. Murray, W.L. Barnes, J. Phys. Chem. C 111 (2007) 11806.
- [35] S. Szunerits, M.R. Das, R. Boukherroub, J. Phys. Chem. C 12 (2008) 8239–8243.
- [36] A. Akjouj, G. Léveque, S. Szunerits, Y. Pennec, B. Djafari-Rouhani, R. Boukherroub, L. Dobrzynski, Surf. Sci. Rep. 68 (2013) 1–67.
- [37] A.V. Whitney, J.W. Elam, S. Zou, A.V. Zinovev, P.C. Stair, G.C. Schatz, R.P. Van Duyne, J. Phys. Chem. B 109 (2005) 20522.
- [38] O. Saison-Francioso, G. Leveque, R. Boukherroub, S. Szunerits, A. Akjouj, J. Phys. Chem. C 119 (2015) 28551–28559.